Journal of Materials Chemistry A

ROYAL SOCIETY OF CHEMISTRY

COMMUNICATION

View Article Online
View Journal | View Issue

Cite this: J. Mater. Chem. A, 2023, 11, 4957

Received 24th December 2022
Accepted 19th January 2023

DOI: 10.1039/d2ta09993d

rsc.li/materials-a

Macrocyclization-induced phosphorescence enhancement of pyridinium-based macrocycles†

Shuo Li,‡[ab] Zhi-Yuan Zhang,‡[a] Jing-Fang Lv,[a] Ling Li,[a] Jian Li[c] and Chunju Li*[a]

Organic room temperature phosphorescence (RTP) has exhibited various applications in optoelectronics and photobiology. Reported here is an effective phosphorescence enhancement strategy through the macrocyclization of phosphorescent pyridine/pyridinium units by methylene linkers. A pyridine macrocycle was synthesized by the condensation of the 3,5-bis(2,4-dimethoxyphenyl)pyridine monomer with paraformaldehyde under the catalysis of a Lewis acid. The methylation reaction of the pyridine macrocycle with methyl iodide and subsequent ion exchange with ammonium hexafluorophosphate and tetrabutyl ammonium halide gave pyridinium macrocycles. Compared with pyridinium monomers, the macrocycles exhibited enhanced phosphorescence with up to 59-fold prolonging of lifetime and 3.7-fold increase of quantum yields. A mechanism study revealed that macrocyclization restrained the rotation/vibration of luminescent units and therefore suppressed nonradiative decay. Moreover, the macrocyclization slowed down the nonradiative and radiative decay processes of the triplet state. Such macrocyclization-induced phosphorescence enhancement (MIPE) would provide a novel and general strategy for enhancing organic room temperature phosphorescence (RTP) and find wide applications beyond phosphorescence.

Introduction

Organic room-temperature phosphorescence (RTP) has shown great promise in the applications of bioimaging,[1–5] optoelectronics,[6–8] data encryption,[9–14] *etc.* It also has great advantages of high molecular diversity, good biocompatibility and low cost compared with inorganics. Therefore, much effort has been devoted to organic RTP. In general, three key factors should be considered for realizing organic RTP with long lifetime, high efficiency and robustness: boosting intersystem crossing (ISC) to produce more triplet state population, stabilizing triplet states and lowering the radiative/nonradiative decays, and shielding luminescent units against quenchers such as oxygen and impurities. Hitherto, notable methods have been reported for pursuing high performance organic RTP. The common strategies to boost the ISC process are to incorporate n-electron groups (*e.g.*, halogens and heteroatoms) or charge transfer states into the luminescent motif,[15–20] which help to realize efficient RTP, especially when these phosphors are restrained by rigid environments such as those resulting from polymerization,[21–26] crystallization,[27–33] matrix rigidification,[34–43] host–guest complexation and supramolecular assembly.[44–46] However, these n-electron groups accelerate radiative decay of triplet excitons; most of the RTP molecules featuring charge transfer tend to undergo a distinct structure transformation in the excited state transition process, thereby resulting in limited suppression of the non-radiative decay of triplet excitons. Thus, it is significant to develop a new strategy for efficient RTP enhancement in the presence of n-electron groups or charge transfer, which will provide new guidelines to design smart luminescent materials.

Our recent studies have demonstrated a good phosphorescent precursor, phenylpyridinium.[47,48] We anticipated that the macrocyclization of the phenylpyridinium units through methylenes would enhance the phosphorescence. Such phosphorescence enhancement is reasonable since the methylenes can restrict vibration and rotation of phosphorescent units by locking them into the skeleton of the macrocycle and therefore suppress nonradiative decay. Moreover, the unconjugated structure of methylene will not disturb the emission of phosphorescent units. Herein, we designed and synthesized pyridine/pyridinium-based macrocycles PC and PC^{2+}, using our

[a]Tianjin Key Laboratory of Structure and Performance for Functional Molecules, College of Chemistry, Tianjin Normal University, Tianjin 300387, P. R. China. E-mail: cjli@shu.edu.cn

[b]School of Advanced Study, Taizhou University, Taizhou 318000, Zhejiang, P. R. China

[c]School of Chemistry and Chemical Engineering, Henan Normal University, P. R. China

† Electronic supplementary information (ESI) available. CCDC 2169350–2169354 and 2065557. For ESI and crystallographic data in CIF or other electronic format see DOI: https://doi.org/10.1039/d2ta09993d

‡ The authors contributed equally to this work.

synthetic method for functional biphen[*n*]arenes.[49,50] All these macrocycles exhibited prolonged phosphorescence lifetime and improved quantum efficiencies in comparison with their monomers, thus exhibiting macrocyclization-induced phosphorescence enhancement (MIPE). Single crystal X-ray diffraction analysis and photophysical characterization revealed that this enormous enhancement is because of the restriction of the macrocyclic skeleton for the phosphorescent units which efficiently suppressed the radiative decay of the singlet state and triplet state, and nonradiative decay of the triplet state.

Results and discussion

First, we examined the synthesis of a pyridine-based macrocycle PC (Scheme 1). As the most commonly used reaction conditions for synthesizing functional biphen[*n*]arenes,[51] a $BF_3 \cdot Et_2O$ catalyst and dichloromethane (DCM) solvent were chosen to achieve the condensation of the monomer PM and paraformaldehyde, giving the cyclic product PC in 15% yield. PC was confirmed by ^1H, ^{13}C NMR, and HRMS (Fig. S1–S6†). The fairly low yield spurred us to screen out good reaction conditions by evaluating solvents, catalysts and the reaction time. As illustrated in Table S1,† chloroform ($CHCl_3$) gave highest yield of 37% for $BF_3 \cdot Et_2O$ and 1,2-dichloroethane (DCE) gave the highest yield of 65% for the trifluoromethanesulfonic acid (TfOH) catalyst after screening DCM, $CHCl_3$, DCE and CH_3CN solvents (entries 1–8). Then $FeCl_3$, $AlCl_3$, $BF_3 \cdot Et_2O$, and TfOH catalysts were studied in DCE and TfOH was proved to be the best (entries 3, 7, 9, and 10). Therefore, the optimized conditions (DCE as the solvent, TfOH as the catalyst, and at 25 °C) were utilized for large-scale preparation (Schemes S1 and S2†). Cationic macrocycle PC·2I was synthesized by methylation of PC with excess CH_3I and recrystallization from EtOH. After the anion exchange of NH_4PF_6, tetrabutylammonium bromide (TBAB) and tetrabutylammonium chloride (TBAC), another two pyridinium macrocycles with counterions of Br^- (PC·2Br) and Cl^- (PC·2Cl) were successfully obtained (Scheme S3 and Fig. S7–S12†). Moreover, the monomers PM·X (PM·Cl and PM·Br) were synthesized using similar procedures (Scheme S4 and Fig. S13–S18†). Single crystal X-ray diffraction analysis revealed the box-like cavity structure of PC with a size of 6.2 Å × 7.0 Å (Fig. 1a, b and Table S2†). Dimethoxyphenyl paralleled with the opposite one and was perpendicular to the adjacent one. Surface electrostatic potential maps showed that this macrocycle possessed a relatively electronegative cavity (Fig. 1e). PC·2Cl has a similar box-like shape and size (6.3 Å × 7.0 Å) compared with PC (Fig. 1c, d and Table S3†). The 0.1 Å increase in size probably arises from the difference of torsion angles. As illustrated in Fig. 3b and S19b,† the torsion angles between central pyridine/pyridinium units and dimethoxyphenyl units are 47°, 49°, 51°, and 54°for PC·2Cl and 65°, 42°, 42°, and 65° for PC. The entire molecule exhibited an obviously more positive surface electrostatic potential than neutral PC (Fig. 1f).

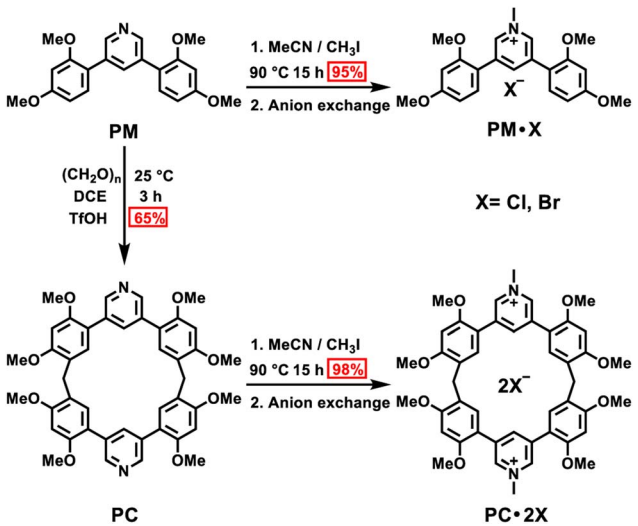

Scheme 1 The synthetic route of monomer PM·X and macrocycles PC·2X.

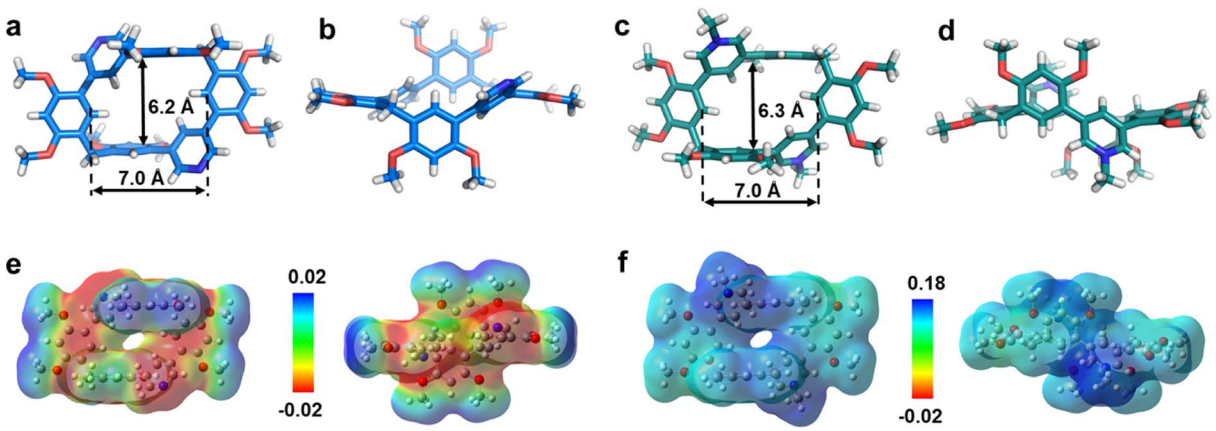

Fig. 1 Single-crystal structures of (a) and (b) PC and (c) and (d) PC·2Cl (top view and side view) and electrostatic potential maps of (e) PC and (f) PC·2Cl (top view and side view). Note: red region represents a low potential area with the characterization of an abundance of electrons. Blue region represents a high potential area with the characterization of a relative absence of electrons. C, marine blue or green; O, red; N, blue; H, white. Counter anions of Cl^- are omitted for clarity.

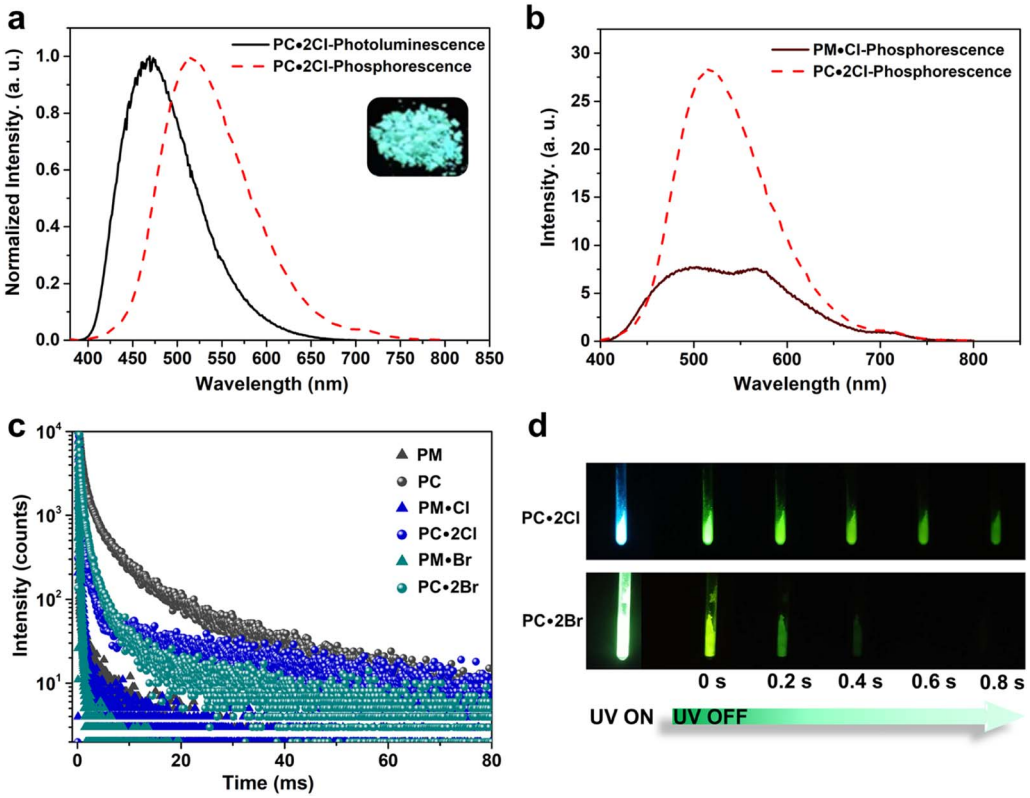

Fig. 2 Photophysical properties of PC, and PC·2X in the solid state. (a) Normalized photoluminescence (solid black line) and phosphorescence spectra (dashed red line) of PC·2Cl under 350 nm excitation (inset: photograph of PC·2Cl under a 365 nm UV lamp). (b) Phosphorescence spectra of PM·Cl (deep red) and PC·2Cl (red) under 350 nm excitation. (c) Lifetimes of macrocycles (PC, PC·2Cl, and PC·2Br) and monomers (PM, PM·Cl, and PM·Br) in the solid state at room temperature. (d) Luminescence photographs of PC·2Cl and PC·2Br under 365 nm light at 77 K and at different time intervals after ceasing irradiation.

The photoluminescence (PL) spectra, phosphorescence spectra and time-resolved spectra were measured to illustrate the effect of macrocyclization on photophysical properties at room temperature. Both monomer PM·Cl and macrocycle PC·2Cl exhibited a cyan emission peak at 470 nm with nanosecond-scale lifetimes in the solid state (Fig. 2a, b and S20, S21†). The phosphorescence spectra revealed that PM·Cl displayed a maximal RTP peak around 500 nm with a lifetime of 0.29 ms, along with a shoulder peak at 565 nm. For the macrocycle PC·2Cl, it showed RTP bands at 518 nm with a lifetime of 16.7 ms (Fig. 2b–d). Significantly, compared with the monomer, macrocycle PC·2Cl showed a 58-fold improvement in the phosphorescence lifetime. Moreover, an enhanced phosphorescence intensity (3.7 fold) was observed in the phosphorescence spectra (Fig. 2b). Actually, PC·2Cl also exhibited higher RTP efficiency than PM·Cl (Fig. S22 and S23†). The above results indicated that the macrocyclization strategy is highly effective in promoting RTP.

Next, PC^{2+} with a bromide counterion and the neutral macrocycle PC were evaluated. PC·2Br ($\lambda_{max} = 481$ nm and $\tau_F = 8.0$ ns) displayed red-shifted emission and prolonged lifetimes compared to PM·Br ($\lambda_{max} = 470$ nm and $\tau_F = 5.6$ ns) (Fig. S24 and S25†). Compared with PM·Br, both phosphorescence lifetime and quantum efficiency of PC·2Br exhibited a prominent enhancement. The lifetime prolonged from 0.15 ms of PM·Br to 7.0 ms of PC·2Br, a 47-fold improvement (Fig. 2c). The phosphorescence intensity also showed 8.3-fold improvement (Fig. S24c†). Similarly, the phosphorescence efficiency improved from 5.9% of the monomer to 7.2% of the macrocycle (Fig. S26b and S27b†). Moreover, the neutral macrocycle PC also showed such MIPE. The monomer PM emitted blue fluorescence ($\lambda_{max} = 338$ nm) with a lifetime of 0.85 ns (Fig. S28†). PC showed a red-shifted emission band at 355 nm with a lifetime of 0.91 ns, accompanied by a shoulder peak at 458 nm (Fig. S29†). The phosphorescence spectra gave a 2.6-fold improvement in intensity (Fig. S29c†). Time-resolved PL decay indicated a prolonged lifetime (10.9 ms for PC and 2.10 ms for PM) (Fig. 2c). This phosphorescence enhancement was also confirmed by improved quantum efficiencies of PC (3.3%) compared with those of PM (1.8%) (Fig. S30 and S31†). Furthermore, a green afterglow could be observed for both PC·2Cl and PC·2Br after ceasing the UV irradiation at 77 K (Fig. 2d). Phosphorescence spectra also showed enormous enhancements as the temperature decreased from 298 K to 77 K (Fig. S32a and b†). Moreover, their lifetimes prolonged from 16.7 ms of PC·2Cl and 7.00 ms of PC·2Br to 241 ms and 51.2 ms, respectively, proving that lowering temperature is beneficial for the phosphorescence intensity and lifetime, which is a typical characteristic of phosphorescent compounds (Fig. S32c and d†). These remarkable enhancements of phosphorescence for all macrocycles (PC,

Table 1 Photophysical data of PM, PC, PM·X, and PC·2X

Entry	Compound	λ_F (nm)	λ_P (nm)	τ_F (ns)	τ_P (ms)	Φ_F (%)	Φ_P (%)	k_r^{Fa} (s^{-1})	$k_{nr}^{F\,b}$ (s^{-1})	$k_{isc}{}^{c}$ (s^{-1})	k_r^{Pd} (s^{-1})	$k_{nr}^{P\,e}$ (s^{-1})
1	PM	338	495	0.85	2.10	6.1	1.8	7.2×10^7	1.1×10^9	2.1×10^7	8.6	468
2	PC	355	495	0.91	10.9	3.5	3.3	3.8×10^7	1.0×10^9	3.6×10^7	3.0	89
3	PM·Cl	470	500	14.1	0.29	10.4	17.3	7.4×10^6	5.1×10^7	1.2×10^7	597	2.8×10^3
4	PC·2Cl	470	518	9.45	16.7	14.6	18.6	1.5×10^7	7.1×10^7	2.0×10^7	11	49
5	PM·Br	470	503	5.6	0.16	3.9	5.9	7.0×10^6	1.6×10^8	1.0×10^7	369	5.9×10^3
6	PC·2Br	481	522	8.0	7.00	4.2	7.2	5.2×10^6	1.1×10^8	9.0×10^6	10	133

[a] The radiative decay rate constant of fluorescence $k_r^F = \Phi_F/\tau_F$. [b] The singlet state nonradiative decay rate constant of fluorescence $k_{nr}^F = (1 - \Phi_F - \Phi_P)/\tau_F$. [c] The intersystem crossing rate constant $k_{isc} = \Phi_P/\tau_F$. [d] The radiative decay rate constant of phosphorescence $k_r^P = \Phi_P/\tau_P$. [e] The triplet state nonradiative decay rate constant $k_{nr}^P = (1 - \Phi_P)/\tau_P$.

PC·2Cl, and PC·2Br) proved the universality of the MIPE strategy.

On the basis of the obtained photophysical properties, the radiative and nonradiative decay rate constants were calculated following the standard methods (Table 1).[52,53] According to Kasha's rule, an excited molecule usually deactivates to the lowest excited singlet S_1. Then S_1 undergoes three competing decay processes: decay to the ground state S_0 *via* a nonradiative process with a rate constant $k_{nr}^F = (1 - \Phi_F - \Phi_P)/\tau_F$; radiative decay to the S_0 by emitting fluorescence with a rate constant $k_r^F = \Phi_F/\tau_F$; conversion to the triplet state (usually is T_n and then fast decay to the lowest triplet state T_1) *via* intersystem crossing with a rate constant $k_{isc} = \Phi_P/\tau_F$. T_1 can decay to S_0 *via* a radiative process by emitting phosphorescence with a rate constant $k_r^P = \Phi_P/\tau_P$ or a nonradiative process with a rate constant $k_{nr}^P = (1 - \Phi_P)/\tau_P$.

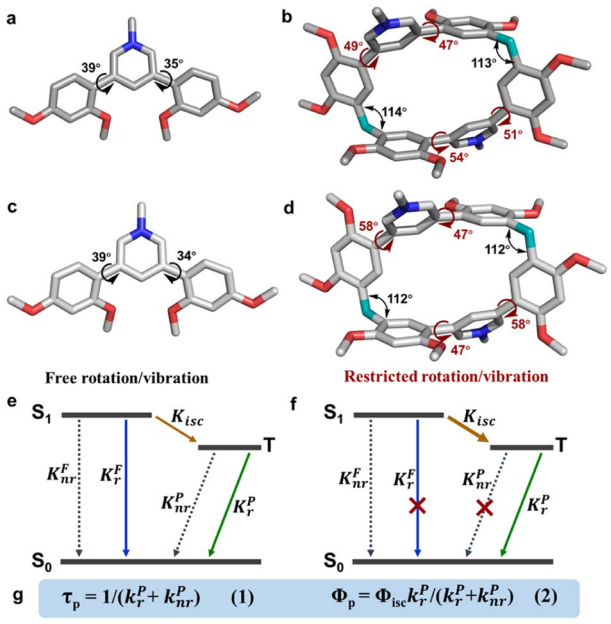

Fig. 3 Mechanism of the macrocyclization strategy for phosphorescence enhancement. The single crystal structures of the monomers (a) PM·Cl and (c) PM·Br and the macrocycles (b) PC·2Cl and (d) PC·2Br. All chloride and bromide ions and hydrogen atoms are omitted for clarity. (e) and (f) Simplified Jablonski diagram of monomers and macrocycles. (g) The equation of τ_P and Φ_P.

The intersystem crossing rate constant is $k_{isc} = (0.9–3.6) \times 10^7$ s^{-1}, which guaranteed the production of sufficient triplet state population. The macrocycles stabilized triplet states and lowered the decay rates of both radiative and nonradiative processes. They jointly provided two indispensable conditions for phosphorescence. The radiative decay rate constant of the triplet state was reduced to $k_r^P = 11$ s^{-1} for PC·2Cl, about 54-fold lower than that of monomer PM·Cl ($k_r^P = 597$ s^{-1}). Such reduction was also found for PC·2Br ($k_r^P = 10$ s^{-1}) and PC ($k_r^P = 3.0$ s^{-1}). Moreover, the nonradiative decay rate constants of the macrocycles ($k_{nr}^P = 49$ s^{-1} for PC·2Cl $k_{nr}^P = 133$ s^{-1} for PC·2Br, and $k_{nr}^P = 89$ s^{-1} for PC) were also much smaller than that of the monomers ($k_{nr}^P = 2.8 \times 10^3$ s^{-1} for PM·Cl, $k_{nr}^P = 5.9 \times 10^3$ s^{-1} for PM·Br, and $k_{nr}^P = 468$ s^{-1} for PM). According to eqn (1) in Fig. 3g, smaller ($k_r^P + k_{nr}^P$) should result in a longer lifetime. These results confirmed that the macrocyclization slowed down the decay of triplet states and favored long phosphorescence lifetime. Moreover, the radiative decay rate constants (k_r^F) of the singlet state were also slightly slowed down after macrocyclization which was beneficial for the ISC and hence probably promoted the phosphorescence enhancement. Eqn (2) indicated that quantum efficiency of phosphorescence Φ_P was dependent on Φ_{isc} and k_{nr}^P/k_r^P. Therefore, the decreased k_{nr}^P/k_r^P (from 4.7 of PM·Cl to 4.5 of PC·2Cl, 16 of PM·Br to 13 pf PC·2Br, and 54 of PM to 30 of PC) means increased $(k_r^P)/(k_r^P + k_{nr}^P)$. The improved Φ_P makes it impossible to confirm the change (increase or decrease) of the Φ_{isc} (Table 1).

Single-crystal X-ray diffraction analysis revealed atomic-level structures for further understanding of such phosphorescence enhancement (Tables S2–S7 and Fig. S33†). As shown in Fig. 3a and b, the torsion angles between pyridinium and dimethoxyphenyls in PM·Cl are 39° and 35°, respectively. Macrocycle PC·2Cl, made up of two PM·Cl and two methylene linkers, has larger torsion angles of 47°, 49°, 51° and 54°. For PC·2Br, the torsion angles are 47° and 58°, larger than those of monomer PM·Br (39° and 34°) (Fig. 3c and d). The increased torsion angles were also found in PC (41° and 52°) and PM (42° and 65°) (Fig. S19†). Because of the definite orientation of methylene, this more twisted structure is the result of structural adjustment after macrocyclization. Rotation of dimethoxyphenyls was prohibited and the vibration was also suppressed because of the restriction of the macrocycle skeleton. As a result, the nonradiative decay processes were greatly restrained and the

radiative decay process was promoted. According to the Jablonski diagram and eqn (1) and (2) in Fig. 3e–g, phosphorescence lifetime $\tau_P = 1/(k_r^P + k_{nr}^P)$ and quantum yield $\Phi_P = \Phi_{isc}k_r^P/(k_r^P + k_{nr}^P)$, the promoted radiative process and decreased $(k_r^P + k_{nr}^P)$ boosted the prolonging of τ_P and improvement of Φ_P and hence phosphorescence enhancement was realized. Furthermore, to thoroughly eliminate the influence of noncovalent interactions ($\pi\cdots\pi$, C–H$\cdots\pi$ interaction, hydrogen bonding, *etc.*) in crystals, the photoluminescence spectra of macrocycle PC·2Cl and monomer PM·Cl in aqueous solution were measured. These noncovalent interactions in the solid state would be completely destroyed by solvation in water and hence reflect the conformation in a free state. Moreover, macrocycle PC·2Cl possessed two monomers of PM·Cl and the photoluminescent spectra of PC·2Cl in a 1×10^{-6} mol L^{-1} solution should be the same as those of PM·Cl in a 2×10^{-6} mol L^{-1} solution if the nonconjugated methylene had no influence on the luminescent units. However, a 4-fold enhancement was observed and proved that the macrocyclization promoted the emission even in solution and the restriction is ever present (Fig. S34†).

To evaluate the intermolecular aggregation, concentration-dependent UV-vis absorption spectra and photoluminescence spectra in an aqueous solution were measured (Fig. S35†). Both the macrocycle and monomer have identical normalized UV-vis absorption spectra, indicating that there is no aggregation which was also confirmed by the identical normalized photoluminescence spectra of PC·2Cl with the concentration changed from 1×10^{-6} to 5×10^{-5} mol L^{-1}. We further evaluated their packing mode in the solid state. Monomers PM·Cl and PM·Br mutually stacked with a typical π–π interaction of 3.56 Å, hinted the H aggregates (Fig. S36 and S37†). However, macrocycles PC·2Cl and PC·2Br stacked to form the tubular superstructures without π–π interactions (Fig. S38 and S39†). Therefore, there are no apparent aggregate modes.[54–57]

Experimental

All reagents and solvents were commercially available and used without further purification, unless otherwise noted. ^{1}H NMR and ^{13}C NMR spectra were recorded using a Bruker Avance 500 MHz spectrometer. High-resolution mass spectra (HRMS) was recorded on an SCIEX, X-500R QTOF instrument. Photoluminescence spectra and lifetime were obtained on an FLS900 and FLS1000. Fluorescence and phosphorescence quantum efficiencies were measured on a HAMAMATSU C9920-02. Melting points were obtained on an X-4 digital melting point apparatus. Single crystal X-ray diffraction data were collected on a Bruker Smart Apex 2 and Bruker D8 Venture. The electrostatic potential maps of PC and PC·2Cl were obtained by using the Gaussian 09 program with B3LYP-D3(BJ)/6-31G+(d,p) and B3LYP-D3(BJ)/6-31G++(d,p) levels, respectively.

Conclusions

In conclusion, we present an effective phosphorescence enhancement strategy of macrocyclization based on pyridine/pyridinium macrocycles. A dimeric pyridine macrocycle was synthesized in 65% yield by the condensation of the 3,5-bis(2,4-dimethoxyphenyl)pyridine monomer and paraformaldehyde under the catalysis of TfOH in DCE. Two pyridinium macrocycles with different counterions were prepared by the methylation of the pyridine macrocycle and subsequent ion exchange in high yields. Significantly, all of them show enhanced phosphorescence compared with monomers. The phosphorescence lifetime increased 59-fold and quantum efficiency showed a 3.7-fold increase after macrocyclization. The mechanism study revealed that the macrocyclic skeleton locked the luminescent units by prohibited rotation and suppressed vibration and therefore suppressed nonradiative decay. Furthermore, the radiative process of the triplet state was also slowed down which favored the improvement of lifetime. This result provided a new strategy and typical examples for realizing organic room temperature phosphorescence with high performance and may promote the development of phosphorescence materials. Considering the universality of this phosphorescence enhancement strategy, more macrocycle-based phosphorescent materials with longer lifetime and higher efficiency will be prepared in the near future.

Author contributions

Chunju Li and Zhi-Yuan Zhang provided facilities and funding and supervised the overall research work. Shuo Li and Zhi-Yuan Zhang designed and conducted experiments, analysis and characterization. Jing-Fang Lv and Ling Li performed mechanism analysis and discussion. All authors discussed the results and commented on the manuscript.

Conflicts of interest

The authors declare no conflict of interest.

Acknowledgements

The authors gratefully acknowledge the National Natural Science Foundation of China (21971192, 21772118, and 22201211), the Natural Science Foundation of Tianjin City (20JCZDJC00200), and Open Research Fund of School of Chemistry and Chemical Engineering, Henan Normal University.

Notes and references

1 G. Zhang, G. M. Palmer, M. W. Dewhirst and C. L. Fraser, *Nat. Mater.*, 2009, **8**, 747.
2 X. Zhen, C. Xie and K. Pu, *Angew. Chem., Int. Ed.*, 2018, **57**, 3938.
3 Y. Wang, H. Gao, J. Yang, M. Fang, D. Ding, B. Z. Tang and Z. Li, *Adv. Mater.*, 2021, **33**, 2007811.
4 W.-L. Zhou, Y. Chen, Q. Yu, H. Zhang, Z.-X. Liu, X.-Y. Dai, J.-J. Li and Y. Liu, *Nat. Commun.*, 2020, **11**, 4655.
5 M. Cui, P. Dai, J. Ding, M. Li, R. Sun, X. Jiang, M. Wu, X. Pang, M. Liu, Q. Zhao, B. Song and Y. He, *Angew. Chem., Int. Ed.*, 2022, **61**, e202200172.

6 S. Hirata, K. Totani, T. Yamashita, C. Adachi and M. Vacha, *Nat. Mater.*, 2014, **13**, 938.
7 R. Kabe, N. Notsuka, K. Yoshida and C. Adachi, *Adv. Mater.*, 2016, **28**, 655.
8 X. Wu, C.-Y. Huang, D.-G. Chen, D. Liu, C. Wu, K.-J. Chou, B. Zhang, Y. Wang, Y. Liu, E. Y. Li, W. Zhu and P.-T. Chou, *Nat. Commun.*, 2020, **11**, 2145.
9 S. Xu, R. Chen, C. Zheng and W. Huang, *Adv. Mater.*, 2016, **28**, 9920.
10 K. Jiang, Y. Wang, C. Cai and H. Lin, *Chem. Mater.*, 2017, **29**, 4866.
11 K. Jiang, Y. Wang, X. Gao, C. Cai and H. Lin, *Angew. Chem., Int. Ed.*, 2018, **57**, 6216.
12 L. Gu, H. Shi, L. Bian, M. Gu, K. Ling, X. Wang, H. Ma, S. Cai, W. Ning, L. Fu, H. Wang, S. Wang, Y. Gao, W. Yao, F. Huo, Y. Tao, Z. An, X. Liu and W. Huang, *Nat. Photonics*, 2019, **13**, 406.
13 A. Abdollahi, H. Roghani-Mamaqani, B. Razavi and M. Salami-Kalajahi, *ACS Nano*, 2020, **14**, 14417.
14 J. Tan, Q. Li, S. Meng, Y. Li, J. Yang, Y. Ye, Z. Tang, S. Qu and X. Ren, *Adv. Mater.*, 2021, **33**, 2006781.
15 R. Kabe and C. Adachi, *Nature*, 2017, **550**, 384.
16 P. Alam, N. L. C. Leung, J. Liu, T. S. Cheung, X. Zhang, Z. He, R. T. K. Kwok, J. W. Y. Lam, H. H. Y. Sung, I. D. Williams, C. C. S. Chan, K. S. Wong, Q. Peng and B. Z. Tang, *Adv. Mater.*, 2020, **32**, 2001026.
17 P. Alam, T. S. Cheung, N. L. C. Leung, J. Zhang, J. Guo, L. Du, R. T. K. Kwok, J. W. Y. Lam and Z. Zeng, *J. Am. Chem. Soc.*, 2022, **144**, 3050.
18 Z. Yang, C. Xu, W. Li, Z. Mao, X. Ge, Q. Huang, H. Deng, J. Zhao, F. L. Gu, Y. Zhang and Z. Chi, *Angew. Chem., Int. Ed.*, 2020, **59**, 17451.
19 G. Farias, C. A. M. Salla, M. Aydemir, L. Sturm, P. Dechambenoit, F. Durola, B. d. Souza, H. Bock, A. P. Monkman and I. H. Bechtold, *Chem. Sci.*, 2021, **12**, 15116.
20 W. Dai, X. Niu, X. Wu, Y. Ren, Y. Zhang, G. Li, H. Su, Y. Lei, J. Xiao, J. Shi, B. Tong, Z. Cai and Y. Dong, *Angew. Chem., Int. Ed.*, 2022, **61**, e202200236.
21 M. S. Kwon, Y. Yu, C. Coburn, A. W. Phillips, K. Chung, A. Shanker, J. Jung, G. Kim, K. Pipe, S. R. Forrest, J. H. Youk, J. Gierschner and J. Kim, *Nat. Commun.*, 2015, **6**, 8947.
22 N. Gan, H. Shi, Z. An and W. Huang, *Adv. Funct. Mater.*, 2018, **28**, 1802657.
23 X. Ma, C. Xu, J. Wang and H. Tian, *Angew. Chem., Int. Ed.*, 2018, **57**, 10854.
24 L. Gu, H. Wu, H. Ma, W. Ye, W. Jia, H. Wang, H. Chen, N. Zhang, D. Wang, C. Qian, Z. An, W. Huang and Y. Zhao, *Nat. Commun.*, 2020, **11**, 944.
25 X. Lin, J. Wang, B. Ding, X. Ma and H. Tian, *Angew. Chem., Int. Ed.*, 2021, **60**, 3459.
26 S. Cai, Z. Sun, H. Wang, X. Yao, H. Ma, W. Jia, S. Wang, Z. Li, H. Shi, Z. An, Y. Ishida, T. Aida and W. Huang, *J. Am. Chem. Soc.*, 2021, **143**, 16256.
27 W. Z. Yuan, X. Y. Shen, H. Zhao, J. W. Y. Lam, L. Tang, P. Lu, C. Wang, Y. Liu, Z. Wang, Q. Zheng, J. Z. Sun, Y. Ma and B. Z. Tang, *J. Phys. Chem. C*, 2010, **114**, 6090.
28 Y. Gong, Y. Tan, H. Li, Y. Zhang, W. Yuan, Y. Zhang, J. Sun and B. Z. Tang, *Sci. China: Chem.*, 2013, **56**, 1183.
29 Z. An, C. Zheng, Y. Tao, R. Chen, H. Shi, T. Chen, Z. Wang, H. Li, R. Deng, X. Liu and W. Huang, *Nat. Mater.*, 2015, **14**, 685.
30 Y. Shoji, Y. Ikabata, Q. Wang, D. Nemoto, A. Sakamoto, N. Tanaka, J. Seino, H. Nakai and T. Fukushima, *J. Am. Chem. Soc.*, 2017, **139**, 2728.
31 Q. Li and Z. Li, *Acc. Chem. Res.*, 2020, **53**, 962.
32 J.-X. Wang, Y.-G. Fang, C.-X. Li, L.-Y. Niu, W.-H. Fang, G. Cui and Q.-Z. Yang, *Angew. Chem., Int. Ed.*, 2020, **59**, 10032.
33 B. Roy, I. Maisuls, J. Zhang, F. C. Niemeyer, F. Rizzo, C. Wölper, C. G. Daniliuc, B. Z. Tang, C. A. Strassert and J. Voskuhl, *Angew. Chem., Int. Ed.*, 2022, **61**, 202111805.
34 M. Baroncini, G. Bergamini and P. Ceroni, *Chem. Commun.*, 2017, **53**, 2081.
35 R. Gao and D. Yan, *Chem. Sci.*, 2017, **8**, 590.
36 Y. Su, S. Z. F. Phua, Y. Li, X. Zhou, D. Jana, G. Liu, W. Q. Lim, W. K. Ong, C. Yang and Y. Zhao, *Sci. Adv.*, 2018, **4**, eaas9732.
37 S. Kuila and S. J. George, *Angew. Chem., Int. Ed.*, 2020, **59**, 9393.
38 Y. Lei, W. Dai, J. Guan, S. Guo, F. Ren, Y. Zhou, J. Shi, B. Tong, Z. Cai, J. Zheng and Y. Dong, *Angew. Chem., Int. Ed.*, 2020, **59**, 16054.
39 B. Chen, W. Huang, X. Nie, F. Liao, H. Miao, X. Zhang and G. Zhang, *Angew. Chem., Int. Ed.*, 2021, **60**, 16970.
40 Z.-A. Yan, X. Lin, S. Sun, X. Ma and H. Tian, *Angew. Chem., Int. Ed.*, 2021, **60**, 19735.
41 Z. Xie, X. Zhang, H. Wang, C. Huang, H. Sun, M. Dong, L. Ji, Z. An, T. Yu and W. Huang, *Nat. Commun.*, 2021, **12**, 3522.
42 Y. Zhang, L. Gao, X. Zheng, Z. Wang, C. Yang, H. Tang, L. Qu, Y. Li and Y. Zhao, *Nat. Commun.*, 2021, **12**, 2297.
43 X. Yan, H. Peng, Y. Xiang, J. Wang, L. Yu, Y. Tao, H. Li, W. Huang and R. Chen, *Small*, 2022, **18**, 2104073.
44 X. Ma, J. Wang and H. Tian, *Acc. Chem. Res.*, 2019, **52**, 738.
45 X.-K. Ma, W. Zhang, Z. Liu, H. Zhang, B. Zhang and Y. Liu, *Adv. Mater.*, 2021, **33**, 2007476.
46 S. Garain, B. C. Garain, M. Eswaramoorthy, S. K. Pati and S. J. George, *Angew. Chem., Int. Ed.*, 2021, **60**, 19720.
47 Z.-Y. Zhang, Y. Chen and Y. Liu, *Angew. Chem., Int. Ed.*, 2019, **58**, 6028.
48 Z.-Y. Zhang and Y. Liu, *Chem. Sci.*, 2019, **10**, 7773.
49 Z.-Y. Zhang and C. Li, *Acc. Chem. Res.*, 2022, **55**, 916.
50 S. Li, K. Liu, X.-C. Feng, Z.-X. Li, Z.-Y. Zhang, B. Wang, M. Li, Y.-L. Bai, L. Cui and C. Li, *Nat. Commun.*, 2022, **13**, 2850.
51 K. Xu, Z.-Y. Zhang, C. Yu, B. Wang, M. Dong, X. Zeng, R. Gou, L. Cui and C. Li, *Angew. Chem., Int. Ed.*, 2020, **59**, 7214.
52 C. C. Byeon, M. M. McKerns, W. Sun, T. M. Nordlund, C. M. Lawson and G. M. Gray, *Appl. Phys. Lett.*, 2004, **84**, 5174.
53 P. C. Y. Chow, S. Albert-Seifried, S. Gélinas and R. H. Friend, *Adv. Mater.*, 2014, **26**, 4851.
54 J. Vollbrecht, *New J. Chem.*, 2018, **42**, 11249–11254.
55 S. Ma, S. Du, G. Pan, S. Dai, B. Xu and W. Tian, *Aggregate*, 2021, **2**, e96.
56 A. Eisfeld and J. S. Briggs, *Chem. Phys.*, 2006, **324**, 376–384.
57 F. Würthner, T. E. Kaiser and C. R. Saha-Möller, *Angew. Chem., Int. Ed.*, 2011, **50**, 3376–3410.

